Vacuum 109 (2014) 333–340

Contents lists available at ScienceDirect

Vacuum

journal homepage: www.elsevier.com/locate/vacuum

Heat transfer and fluid characteristics of rarefied flow in thermal cavities

Ehsan Yazdanpanah Moghadam [a], Ehsan Roohi [a, *], Javad Abolfazli Esfahani [b]

[a] High Performance Computing Laboratory, Department of Mechanical Engineering, Faculty of Engineering, Ferdowsi University of Mashhad, P.O. Box 91775-1111, Mashhad, Iran
[b] Center of Excellence on Modeling and Control Systems (CEMCS) & Department of Mechanical Engineering, Ferdowsi University of Mashhad, P.O. Box 91775-1111, Mashhad, Iran

ARTICLE INFO

Article history:
Received 3 February 2014
Received in revised form
2 June 2014
Accepted 8 June 2014
Available online 17 June 2014

Keywords:
DSMC
Thermal cavity
Rarefied flow
Thermal creep
Vortical flow
Heat flux
MEMS

ABSTRACT

In the present study, we investigate the characteristics of thermal cavities in the rarefied flow regime using the Direct Simulation Monte Carlo (DSMC). We use a recently developed iterative technique to impose a desired wall heat flux boundary condition in the DSMC algorithm. Fluid mechanics and heat transfer behavior are studied over the walls and in the domain of the thermal cavity over a wide range of Knudsen number in the slip and transition regimes. The vortice behavior is described at different Knudsen numbers in detail. We numerically justify unconventional flow movement from the cold region to the hot region. Finally, we consider the effects of molecular structural parameters such as molecular mass and degree of freedom on the thermal behavior of the thermal cavity flows.

1. Introduction

In recent years, small-scale electromechanical systems have been widely employed in many practical applications including mechanical and engineering biomedical devices. In this regards, a true understanding of the hydrothermal behavior of rarefied flow is required for an optimal design, operation, and manufacturing of these devices [1]. Advances in the development of high density power electronics, heat recovery and high temperature power has led to the development of high temperature heat exchangers (HTHE) with temperatures as high as 2500 K [2]. Investigating thermal conditions in small-scale systems due to high power densities requires the application of efficient techniques to predict allowable performance limits of these systems [3]. As the gas density reduces, Knudsen number (Kn), defined as the ratio of the mean free path of gas molecules to the characteristic length of the flow domain, $Kn = \lambda/L$, increases and the flow analysis must be performed using accurate approaches based on gas kinetic theory [4]. A well-established classification of the gas flow regimes exists according to Kn range [5]: continuum regime ($Kn < 0.001$), slip flow regime ($0.001 < Kn < 0.1$), transition flow regime ($0.1 < Kn < 10$), and free molecular regime ($Kn \geq 10$). Direct simulation Monte Carlo (DSMC) is widely employed to model flow fields in all degrees of flow rarefaction [6].

The aim of this study is to simulate rarefied flow in thermal cavity geometries with an imposed heat flux on the bottom wall. This small-scale thermal cavity represents devices such as a Pirani gauge [7] or a cantilever heater [8]. The rarefied gas flow behaviors in the thermal cavity with constant wall temperature have been studied in the literature. For example, Papadopoulos et al. [9] used direct simulation Monte-Carlo method to study characteristics of thermal creep convective motion in a rectangular geometry at $Kn = 0.05$. They found that a vortex is formed by thermal creep at the non-isothermal boundaries; vortex formation was also observed in the absence of gravity. Aoki et al. [10] used kinetic theory to investigate the flow of a rarefied gas caused by a discontinuous wall temperature in a two-dimensional square container. The steady flow in the container was numerically analyzed using the Bhatnagar–Gross–Krook (BGK) model of the Boltzmann equation. They showed that, as the rarefaction effect decreases, the maximum flow speed tends to approach a finite value, but the region with appreciable flow shrinks to the points of discontinuity. Therefore, the overall flow in the container vanishes non-uniformly in the continuum limit. Sone et al. [11] introduced

* Corresponding author. Tel.: +98 511 8805136; fax: +98 511 8763304.
E-mail address: e.roohi@ferdowsi.um.ac.ir (E. Roohi).

http://dx.doi.org/10.1016/j.vacuum.2014.06.009
0042-207X/

various kinds of flows induced by the temperature effects and discussed their physical mechanisms in rarefied gases. They demonstrated that a tangential temperature gradient along the surface could induce the flow movement from the cold to the hot region. This behavior was known as thermal creep that vanishes in the continuum limit. Liu et al. [12] considered heat transfer in the continuum and early transition regimes (Kn = 0.2) in the vacuum package Micro-Electro-Mechanical-Systems (MEMS) devices with constant wall temperature. They concluded that, if the bottom plate temperature partially increases, the gas temperature near the bottom surface would be greater in comparison with the case where the bottom plate temperature is increased uniformly. In addition, they indicated that gravity in low-pressure MEMS packaged devices has little effect on heat transfer. Cia et al. [13] analyzed heat transfer effects in a vacuum package in the free molecular and near continuum regimes. They simulated a square cavity where the bottom plate represents a hot chip and the other plates were set at room temperature. In the free molecular flow regime, the density and temperature were surveyed with a proposed model. They especially concentrated on the free molecular flow and proposed a model that links the number densities reflected on and traveling away from the walls. Rana et al. [14] studied the effects of rarefaction on the heat transfer behavior of square cavity using the regularized 13 moments (R-13) equations. The heat transfer was compared between the classical Navier–Stokes (NS) and R-13 equation with specified wall temperature (SWT) boundary condition at Kn $\leq$ 0.5. They showed that the classical NS equations overestimate the heat transfer in the MEMS packaged device.

In contrast to the NS equations, there is no classical way to implement a specified heat flux distribution on the wall using the DSMC method; however, some MEMS require the specified wall heat flux boundary condition. In such engineering applications, a specified wall heat flux is more common than a specified wall temperature. For example, the Scienta Pirani gauge is divided into two types [7]: constant resistance, and constant current. The constant resistance type changes the supplied current to maintain the resistance of the filament constant. In fact, the temperature variation is calculated according to changing resistance; therefore, we can simulate this type with the SWT boundary condition. However, it should be noted that this requires more complicated electronics to be controlled. The other type, i.e., the constant current type, has a power supply that provides a constant current to the filament continuously. If we use a simple voltage control circuit, we will obtain a constant power Pirani gauge; therefore, this type could be simulated using the wall heat flux boundary condition.

To apply a specified wall heat in the DSMC method, Wang et al. [15,16] introduced an inverse temperature sampling (ITS) technique. More recently, Akhlaghi et al. [17] introduced an iterative technique to impose a desired (positive/negative) wall heat flux boundary condition in the DSMC method. They validated their technique for different sets of geometries. Our literature review shows that previous simulations of rarefied thermal cavities were based on specified wall temperature (SWT) boundaries [9–14]. Simulation of the cavity with wall heat flux boundary condition is not reported in the literature. Therefore, in the current work, we consider flow field and thermal behavior of a thermal cavity with the constant wall heat flux boundary condition over a wide range of Kn, i.e., from the slip to the mid transition regime, i.e., 0.05 < Kn < 3. The effects of the cavity walls on vortices behavior is discussed in detail. The heat flux and temperature distribution is connected to vortice behavior. The shear stress behavior on the walls and in the domain is considered with increasing Kn. We provide a physical description for the flow and thermal field behavior in the thermal cavity geometry. Finally, thermal analysis is presented for various gas molecular structural parameters.

2. Numerical method

2.1. DSMC approach

The DSMC is a particle method based on kinetic theory for simulation of rarefied gases. The method is carried out by modeling the gas flow using many independent simulator particles. More details about the DSMC algorithm were given in Ref. [18]. In the current study, we use and extend the previous codes of Roohi and co-workers [19–26] to simulate rarefied flow in small-scale cavities. More specifically, the numerical algorithm of the cavity solver from Ref. [19] is upgraded to include the iterative technique. The variable hard sphere (VHS) collision model is used as the collision model in all simulations. Collision pairs are chosen based on the no time counter (NTC) method, in which the computational time is proportional to the number of simulator particles [18]. We use the diffuse reflection model with full thermal accommodation for the walls. To satisfy the size limitation, the cell dimensions in both directions are 0.1λ (m), and we set the time step equal to 1×10^{-12} (s), smaller than the mean collision time. For a typical simulation, twenty particles are initially set in each cell to minimize the statistical scatter. In Table 1, cell size, number of particles in each cell, time step, number of time steps, and number of samples are reported.

2.2. The iterative technique

The Iterative technique is a newly-developed method for imposing a wall heat flux in the DSMC algorithm. This technique is based on the correction of the wall temperature during the DSMC simulation to obtain the desired wall heat flux. In this technique, the wall temperature can be obtained from Ref. [17]:

$$T_w(x)^{\text{new}} = T_w(x)^{\text{old}} + \Delta T_w(x) \tag{1}$$

$\Delta T_w(x)$ is defined as a correction value to the wall temperature such that the iterative algorithm converges and the final wall temperature distribution corresponding to the desired heat flux is established. A positive wall heat flux indicates heat being transferred from the gas to the wall, i.e., a cooling process. On the other hand, a negative value indicates that the wall is heating the gas. In the iterative technique, the corrected wall temperature is computed as follows:

$$T_w(x)^{\text{new}} = T_w(x)^{\text{old}} \left(1 + RF \frac{q_w(x) - q_{\text{des}}(x)}{|q_{\text{des}}(x) + \varepsilon_0|}\right) \tag{2}$$

In Eq. (2), q_w is the wall heat flux, computed according to Ref. [18], and ε_0 is a non-zero positive value that is negligible in comparison to the incident energy flux. ε_0 is typically considered a small non-zero value for adiabatic wall cases because Eq. (2) diverges if the desired heat flux (q_{des}) is set zero. RF is a relaxation factor used to avoid divergence during running the program. This amount is considered 0.03 in our simulations.

Table 1
Entry data for the numerical code.

	Cell size ($\text{m} \times 10^{-8}$)	Number of particles in each cell	Time step ($\text{s} \times 10^{-12}$)	Number of time steps to steady state condition ($\times 10^{+6}$)	Sample size ($\times 10^{+6}$)
Typical test cases	1.67	20	1	8	160

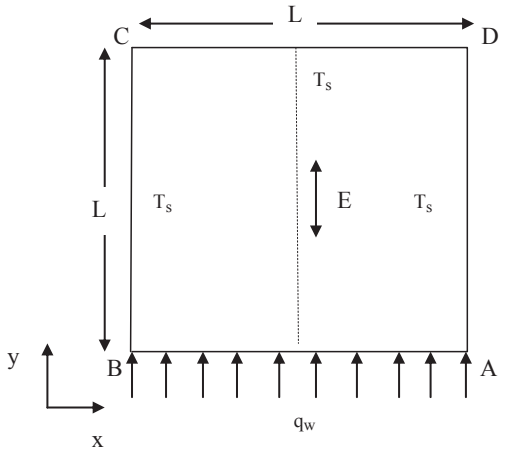

Fig. 1. Geometrical configuration of the cavity.

3. Results and discussion

The thermal cavity considered in this study is shown in Fig. 1. The four corners of the cavity are denoted by A, B, C, and D. The heat flux (positive/negative) is imposed on the bottom wall, and the thermal condition of the three other walls is set as constant temperature, $T_S = 300$ K. Heating and cooling processes have been performed over a wide range of Kn in the slip and transition regimes, i.e., Kn = 0.05, 0.2, 0.5, 1 and 3.

We analyze monatomic argon and diatomic nitrogen molecules. The gas properties are reported in Table 2 [18].

3.1. Grid size/time step independency test

To consider the effects of grid size on the accuracy of the solution, we considered three investigated grids at Kn = 0.2: Grid 1 (72,000 particles in 60 × 60 cells), Grid 2 (200,000 particles in 100 × 100 cells), Grid 3 (450,000 particles in 150 × 150 cells) keeping the number of particles per cell constant at 20. Our simulation showed that the maximum difference between the temperature distribution along line *E* (indicated in Fig. 1) from Grid 1 with that of Grid 3 did not exceed 0.4%. It should be noted that other properties of the gas were also observed invariant with respect to the grid refinement. Therefore, Grid 1 (60 × 60) was selected for the simulations reported in this paper. We also tested different time step sizes and observed that the changes in the temperature distribution over line *E* using $\Delta t = 1 \times 10^{-12}$ (s) and $\Delta t = 1 \times 10^{-13}$ (s) does not go beyond 0.5%. Consequently, a time step of $\Delta t = 1 \times 10^{-12}$ (s) provides a time independent solution. For full validation of the iterative technique, see Ref. [17].

3.2. Heat flux and thermal behavior

We employ the iterative technique to investigate the heat flux and thermal behavior of the cavity. Fig. 2 shows temperature and heat flux contours in the thermal cavities. The imposed heat flux on the bottom wall was set equal to −5 (W/cm^2). This value is selected in such a way that sensible variations for the temperature inside the investigated thermal cavity cases will be obtained. The heat flux and temperature contours and lines reported in this paper are normalized with respect to the desired heat flux ($q_{des} = -5$ W/cm^2) and the wall constant temperature ($T_s = 300$ K), respectively.

Fig. 2 shows that by increasing Kn, the range of heat flux variation between the bottom and the top region decreases. In fact, the increase of Kn results in a lower number of particles inside the domain; therefore, intermolecular and molecule-surface interaction frequency decreases, and penetration of the heat flux from the bottom wall toward the inside of the domain weakens, and heat transfer between adjacent layers reduces. A specified q_y/q_{max} moves far away from the bottom wall as Kn increases, for example $q_y/q_{max} = 0.8$ is located between $y/L = 0.1$ and $y/L = 0.15$ along the line *E* at Kn = 0.05, whereas the location of the constant contour increases to between $y/L = 0.3$ and $y/L = 0.35$ at Kn = 3.

Fig. 2 shows the heat flux behavior directly affects the temperature profiles. At a lower Kn, in contrast to the heat flux distribution, the range of temperature change is smaller. At lower Knudsen numbers, intermolecular and surface-molecules interactions are more frequent. Therefore, the molecules rapidly transfer the gained energy from the bottom wall to the side and top walls, which are the regions with minimum temperature in the cavity; as a result, the range of the temperature variations reduces with the decrease of Knudsen number.

In the next stage, we analyze the heat flux behavior over the cavity surfaces. Once a particle collides with a surface, the energy is transferred in the form of the heat and stress. The imposed heat flux on the bottom wall causes increasing temperature inside the domain, this heat flux transfers to the environment through the other walls, i.e., the cooling process is performed by the side and top walls. Fig. 3 shows the heat flux over the side walls and the top wall for different Knudsen numbers. It is observed that the maximum amount of the heat flux (for the cooling process) arises on the bottom corners of the domain because the largest temperature gradients occur in these regions. Fig. 3 demonstrates that the amount of cooling reaches roughly +6 W/cm^2 on the bottom corner of the side walls (B and A) at Kn = 0.05. This amount is larger than the imposed heat flux on the bottom wall. As these regions have such a great rate of cooling, the amount of heat fluxes on the top side walls (C and D) reaches nearly 0 W/cm^2. When the bottom corner of the side walls performs cooling duty, the upper side walls have a smaller contribution in cooling at Kn = 0. 05. As Kn increases, due to the decrease of intermolecular and molecular-surface interactions, the rate of cooling diminishes on the bottom side walls; therefore, the cooling duty transfers to the upper part of the cavity walls. As Fig. 3 shows, the heat flux on the top parts of the side walls increases and the top wall (CD) contributes more in the cooling process.

3.3. Vortices behavior of the thermal cavity

Fig. 4 shows the structure of flow vortices appearing in the thermal cavity due to the bottom wall heating at different rarefaction regimes. An arrow near to each case shows magnitude of the velocity vectors. At Kn = 0.05, only two vortices are observed over the bottom wall, while the number of vortices increases to four once Kn increases to 0.2. At Kn = 0.2, however, the two vortices located over the bottom wall are smaller than the corresponding vortices at Kn = 0.05 and the other two vortices appear adjacent to the side walls. The vortices located near the bottom wall and side walls rotate in opposite directions.

Table 2
Properties of gases.

Gas	Diameter ($d \times 10^{10}$ m)	Degrees of freedom (ζ)	Molecular mass ($m \times 10^{27}$ kg)	Viscosity index (ω)
Nitrogen(N_2)	4.17	5	46.5	0.74
Argon (Ar)	4.17	3	66.3	0.81

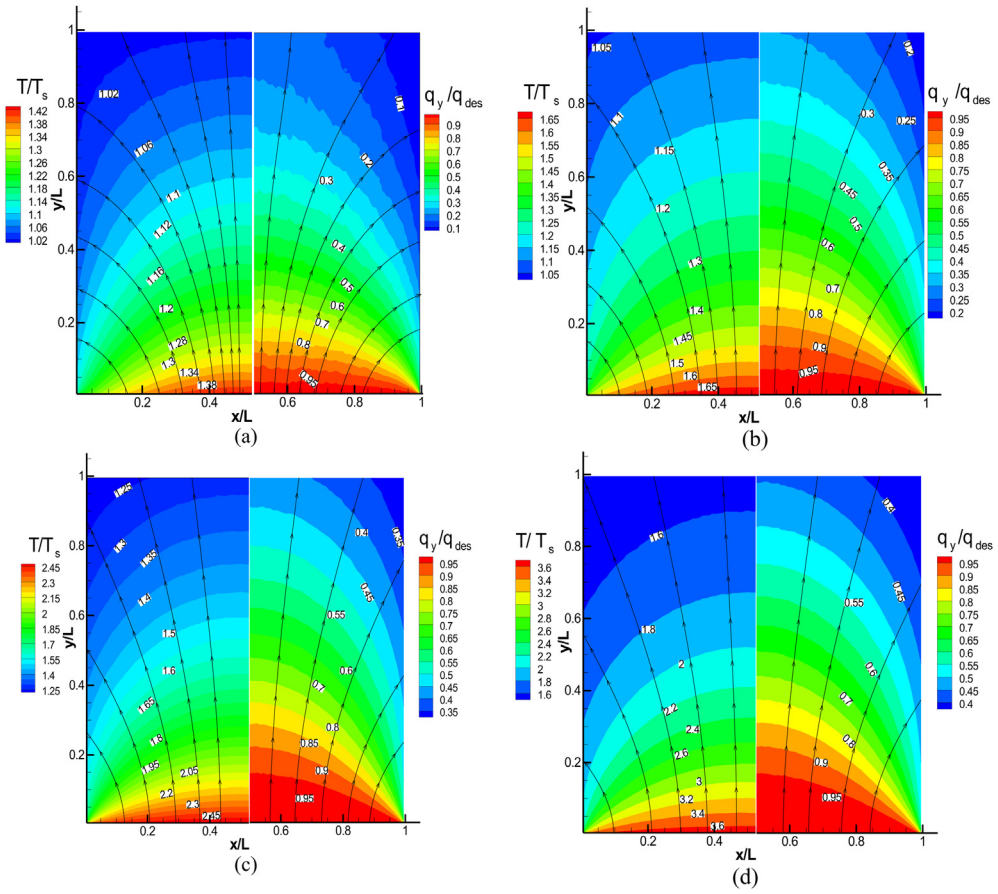

Fig. 2. Heat flux streamlines overlaid on contours of heat flux (right) and temperature (left) (a) Kn = 0.05 (b) Kn = 0.2 (c) Kn = 1 (d) Kn = 3.

These "adjacent to the side walls" vortices are invigorated with the increase of Kn, while the two other vortices over the bottom wall weaken so that these two vortices disappear at Kn = 3. Fig. 4(a)–(c) demonstrates an unconventional behavior different from our observation in the continuum regime, i.e., flow movement from the cold to the hot region over a very small section of the side wall and the bottom wall. This behavior is known as thermal creep [8,25,26].

Rana et al. [14] discussed this behavior and the induced tangential velocity along the side wall using the regularized 13 moment equations (R-13) for Kn $\leq$ 0.5 thermal cavity flows. They concluded that this behavior results from the interplay of some variables that can be described by the R-13 equations [14]. According to the R-13 equations, at small Knudsen numbers, tangential velocity (ϑ_τ) depends on two opposing contributions, i.e., $\vartheta_\tau \propto (\sqrt{\pi\theta/2}\sigma_{\tau n} - 0.2q_\tau)$, where $\theta = RT$, T is the thermodynamic temperature, R is the gas constant, q_τ is the tangential heat flux, and $\sigma_{\tau n}$ is the shear stress. Fig. 5(a) and (b) shows these two terms normalized with respect to $\sqrt{T_0}\sigma_0(\sigma_0 = \rho_0 R T_0)$ and the desired heat flux (q_{des}), respectively, obtained from the current DSMC simulations using microscopic definitions [18]. Fig. 5(c) shows the tangential velocity from the current simulation. According to the above equation, when the second term (q_τ) is greater than the first one ($\sqrt{\pi\theta/2}\sigma_{\tau n}$), the tangential velocity is induced in the negative y-direction over the side wall and via versa.

Fig. 5(d), wall temperature normalized with respect to the maximum temperature inside the domain at each Kn, demonstrates that sharp temperature gradient arises between the center and the two corners of the bottom wall at lower Kn. This produces a force that makes the flow move from the two corners to the center of the bottom wall. The above-described phenomenon leads to the formation of two large vortices over the bottom wall, see Fig. 4. At Kn = 0.05, according to Fig. 5(c), the consequence of the first and second terms is a negative tangential velocity which covers the larger part at the bottom of the side wall in comparison with other Kn cases. At Kn = 0.05, the cooling at the bottom of the side walls is

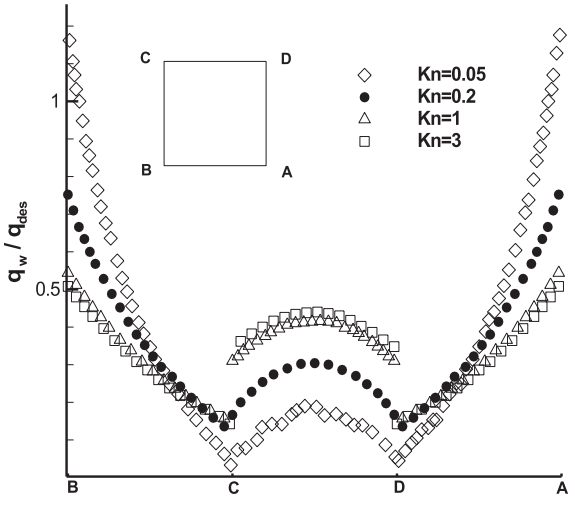

Fig. 3. The heat flux over the top wall and side walls of the cavity.

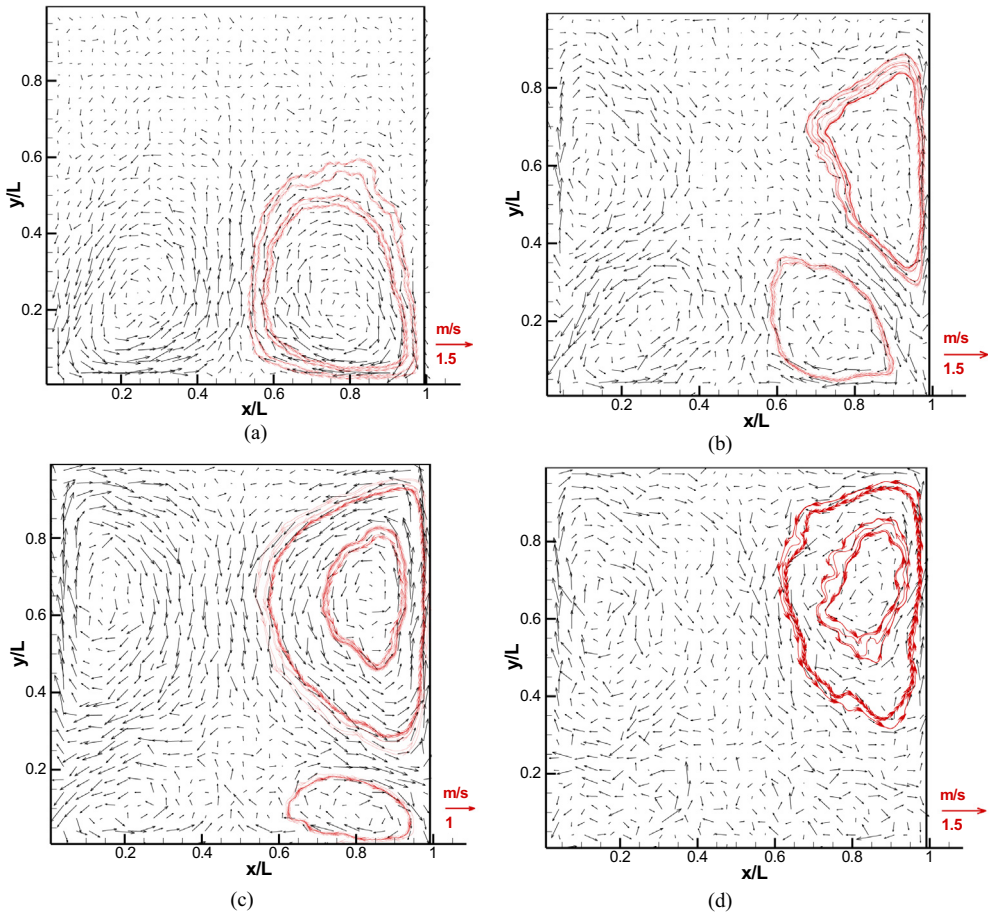

Fig. 4. Velocity streamlines at different Knudsen numbers (a) Kn = 0.05 (b) Kn = 0.2 (c) Kn = 1 (d) Kn = 3 (Note: right hand side vortices are highlighted).

stronger, see Fig. 3; therefore, the top parts of the side walls and the top wall have a low heat flux gradient.

This causes the conductive behavior that governs the top part of the cavity; see Fig. 4(a). Fig. 5(c) confirms this behavior, because the tangential velocity remains almost zero at the upper parts of the side wall.

At Kn = 0.2, Fig. 5(c) shows that, with the exception of a small region, all parts of the side wall induce an upward motion in contrast to Kn = 0.05 case. This causes one vortex to appear over the side wall. At this Kn, the temperature gradient over the bottom wall decreases compared to the Kn = 0.05 case, see Fig 5(d). Therefore, as was shown in Fig. 4(b), two smaller vortices appear over the bottom wall. Fig. 5(d) shows that at Kn = 1, a smaller temperature gradient arises between the center and the two corners of the bottom wall; therefore, the effect of the bottom wall is weakened over the emerging bottom vortices. At Kn = 1, the upward induced force is greater than lower Kn cases, because the tangential velocity at Kn = 1 is higher than other Kn cases; therefore, we expect that two large vortices appear over the side walls, see Fig. 4(c).

Fig. 5(d) shows that the temperature gradient over the bottom wall at Kn = 3 is almost zero; therefore, thermal creep vanishes; as a result, the vortices over the bottom wall disappear. However, the vortices over the side walls appear as the top part of the side walls naturally induce a hot-to-cold flow movement. It should be noted that the thermal creep decreases in spite of the increase of Kn. This is due to the reduction of the heat flux, especially in the two bottom corners of the cavity. Therefore, the temperature gradient over the bottom wall reduces by increasing Kn. It should be noticed that non-zero values of the tangential velocity in cavity corners, as observed in Fig. 5(c), appear only as a result of discretization errors, i.e., finite cell size.

In order to attest our discussion about the induced tangential velocity by the side walls, we set two test cases at Kn = 0.2: first, a cavity with the two adiabatic side walls; second, cavity with an adiabatic top wall. Fig. 6(a) illustrates that there are two elongated vortices extending vertically from the bottom wall to the top wall. The vortices over the side walls vanish, whereas Fig. 6(b) shows that by insulating the top wall, the vortices over the side wall become slightly larger than the vortices shown in Fig. 4(b). Consequently, two side walls play key roles in vortice formation in thermal cavities.

3.4. Heat flux and temperature distribution

Fig. 7 demonstrates that the dimensionless heat flux distribution along the y-direction over the $x = 0.5$ line increases with Kn. At Kn = 0.05, as shown in Fig. 4(a), the two large vortices over the bottom wall cause the imposed heat flux to penetrate deeper compared to other Knudsen numbers, while the conductive behavior on the top part of the cavity obstructs this penetration. By increasing Kn, the vortices over the bottom wall are weakened and the strength of the heat flux penetration is reduced. On the other hand, on the top part of the cavity, the larger vortices appear over the side walls where they transfer heat flux from the side walls and top corners to the center of the top wall. Therefore, the range of

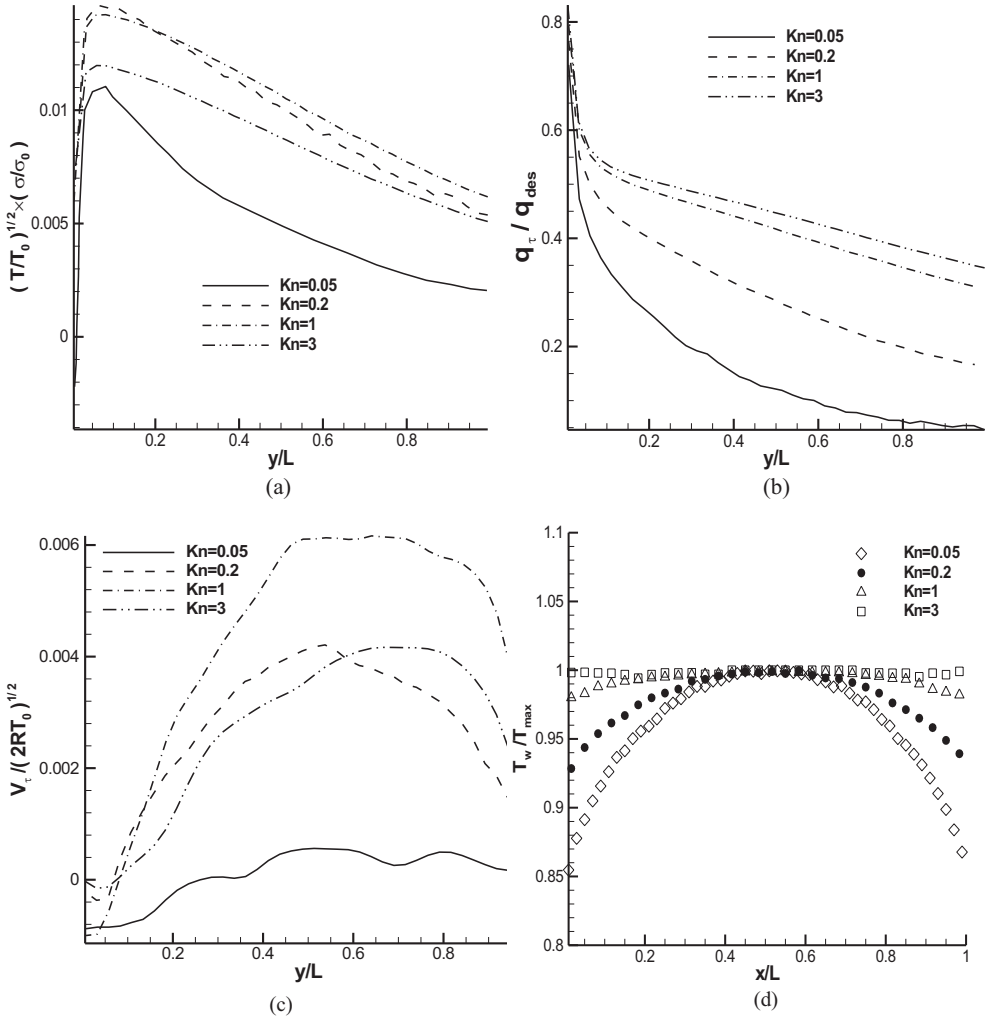

Fig. 5. (a) Non-dimensional first term and (b) second term of the R-13 equation in relation to the tangential induced velocity over the side wall (c) the non-dimensional tangential velocity over the side wall (d) the non-dimensional temperature over the bottom wall.

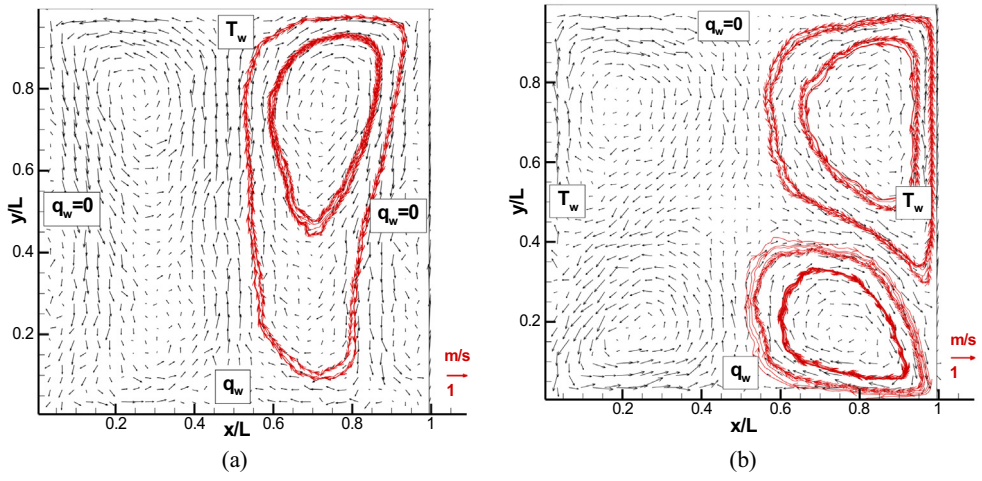

Fig. 6. The effect of wall boundary condition on the vortices over the side wall at Kn = 0.2 (a) the two side walls are adiabatic (b) the top wall is adiabatic.

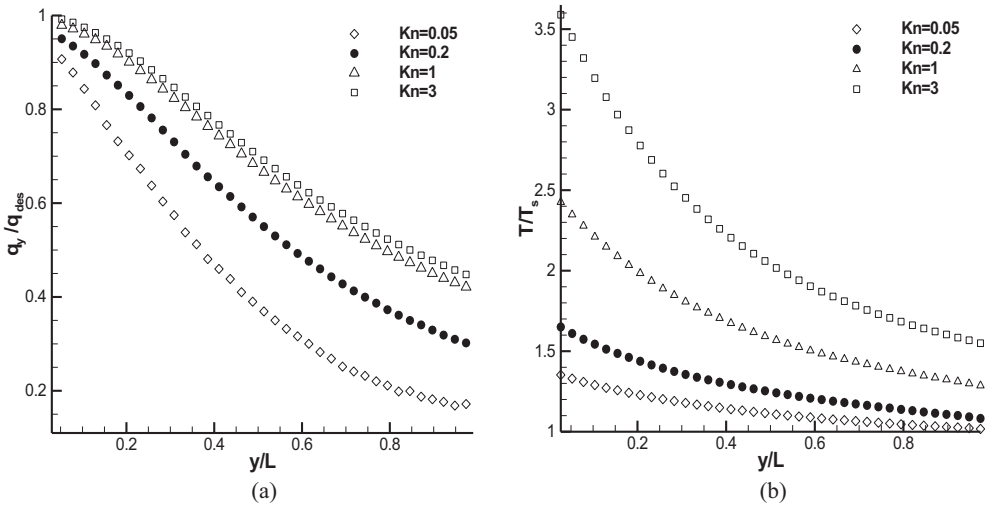

Fig. 7. (a) The non-dimensional heat flux and (b) the temperature distributions along the y direction in the $x = 0.5$.

heat flux variation between the bottom and the top walls becomes larger with the decrease of Kn.

At Kn = 0.05, the temperature variation on the top part of the cavity decreases because there are no vortices which transfer the temperature of the side walls and top wall to the center of the cavity. By increasing Kn, the vortices over the side walls emerge, which causes the thermal energy on the side walls and top wall transfer to the center of the cavity; as a result, the range of temperature variations becomes smaller as Kn decreases.

3.5. The effect of gas molecular structures

In this section, we consider the variation of thermal behavior due to changes in the gas molecular structure in the thermal cavity. The considered gas molecules are monoatomic argon and diatomic nitrogen, see their detailed properties in Table 2.

The relation between the specific heat capacity (C_p), the number of degrees of freedom (ζ) and the gas constant (R) is [18]:

$$C_p = \left(\frac{\xi}{2} + 1\right)R \tag{3}$$

The gas constant R (kJ/kg K) is a function of molecular mass, therefore, the heat capacity depends on two factors: the number of degrees of freedom and molecular mass. The energy of molecules may be stored in translational, rotational, and vibrational modes. The vibrational mode is negligible when the magnitude of the temperature field is very low in comparison with the characteristic temperature of the vibrational mode. The argon atom can only store energy in three translational modes, but the nitrogen molecule possesses two additional rotational modes. On the other hand, argon's mass is larger than nitrogen's; therefore, the heat capacity of nitrogen is greater than argon. It means that if a constant level of energy is transferred to argon and nitrogen molecules, the argon temperature increases more than nitrogen.

Fig. 8(a) illustrates the argon and nitrogen temperature along line E at different Knudsen numbers. The behavior observed in this figure confirms the above discussions, i.e., the argon temperature increases more than that of nitrogen for a constant imposed heat flux at a specified Kn. Fig. 8(b) shows the heat flux behavior of argon and nitrogen along line E. Similar to the temperature, the heat flux of argon is noticeably higher than for nitrogen at each specified Kn.

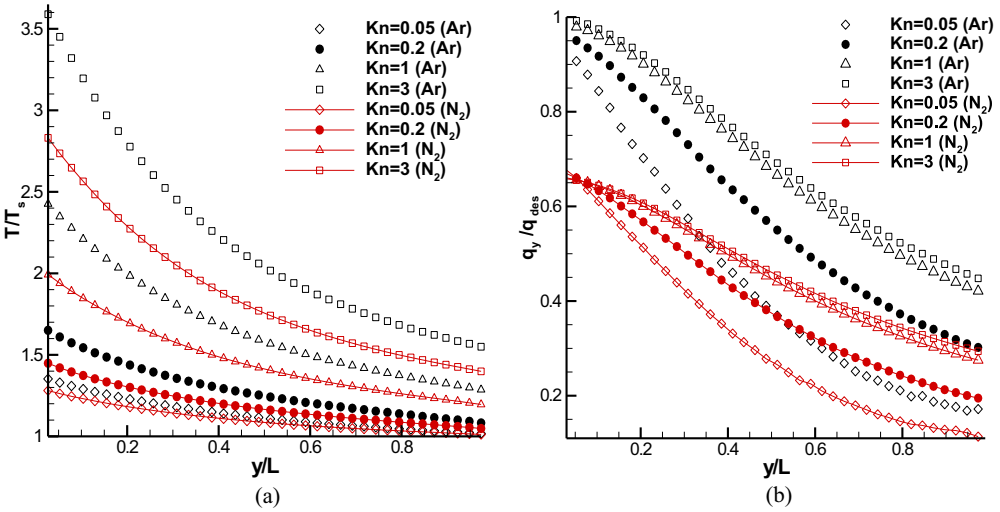

Fig. 8. Comparison of (a) the non-dimensional temperature and (b) the non-dimensional heat flux between the argon and nitrogen at different Kn.

4. Conclusion

The current work investigated the hydrothermal behavior of rarefied flow through cavities using the DSMC technique. We observed that the increase of Kn decreased the intermolecular and molecule-surface interactions; therefore, the penetration of heat transfer inside the cavity weakened and the range of heat flux variation decreased. The vortice behavior over the bottom wall was explained by studying the temperature gradient (thermal creep). By increasing the rarefaction effects, the temperature gradient decreased; therefore, it weakened the two vortices over the bottom wall in such a way that they vanished at $Kn = 3$. On the other hand, the thermal creep induced a tangential velocity along the side walls, which weakened as Kn decreased. To consider the effects of the side walls on vortice formation, we showed that making two side walls adiabatic at $Kn = 0.2$ makes the vortices on the vertical walls disappear. The temperature distribution along the cavity increases with the rise of Kn as a few vortices appear at the top of the cavity. These vortices cause the temperature of the side walls and top wall to be felt at the center of the cavity. On the other hand, the vortices over the bottom wall weakened and the heat flux penetration is reduced. By increasing Kn, the shear stress on the bottom wall decreases in such a way that shear stress is almost zero at $Kn = 3$. The effects of the molecular structures, i.e., mass and degrees of freedom, were investigated on the thermal behavior of the thermal cavity. We observed that the increase of ζ and the decrease of the molecular mass result in a decrease of the temperature and heat flux variation inside the domain.

Acknowledgment

The authors would like to acknowledge financial supports of “Iranian Elite Foundations” for equipping HPC laboratory under Grant No. 100718. The authors would like to acknowledge Prof. Stefan Stefanov from the Bulgarian Academy of Science for helpful discussions during the preparation of this paper. We also would like to thank Dr. Craig White from the Strathclyde University for reading and improving the language of the paper. The authors would also like to acknowledge the reviewers of this paper for their helpful comments that improved the quality of the manuscript.

References

[1] Zhang ZM. Nano/microscale heat transfer. New York: McGraw-Hill; 2007.
[2] Ohadi M, Buckley G. High temperature heat exchangers and microscale combustion systems: applications to thermal system miniaturization. Exp Therm Fluid Sci 2001;25:207–17.
[3] Birur GC, Sur TW, Paris AD, Shakkottai P, Green AA, Haapanen SI. Micro/nano spacecraft thermal control using MEMS-based pumped liquid cooling system. Proc SPIE Microflui BioMEMS 2001;4560:196–206.
[4] Sone Y, Aoki K, Takata S, Sugimoto H, Bobylev AV. Inappropriateness of the heat conduction equation for description of a temperature field of a stationary gas in the continuum limit: examination by an asymptotic analysis and numerical computation of the Boltzmann equation. Phys Fluids 1996;8:628–39.
[5] Kennard EH. Kinetic theory of gases. New York: McGraw-Hill; 1938.
[6] Bird GA. Approach to translational equilibrium in a rigid sphere gas. Phys Fluids 1963;6:1518–9.
[7] Zhang FT, Tang Z, Yu J, Jin RC. A micro-Pirani vacuum gauge based on micro-hotplate technology. Sen Actuators 2006;126:300–5.
[8] Lee J, Wright T, Abel M, Sunden E, Marchenkov A. Thermal conduction from microcantilever heaters in partial vacuum. Appl Phys 2007;101:014906.
[9] Papadopoulos DH, Rosner DE. Enclosure gas flows driven by non-isothermal walls. Phys Fluids 1995;7:2535–7.
[10] Aoki K, Takata S, Aikawa H, Golse F. A rarefied gas flow caused by a discontinuous wall temperature. Phys Fluids 2001;13:2645–61.
[11] Sone Y. Flow induced by temperature fields in a rarefied gas in the continuum limit. Annu Rev Fluid Mech 2000;32:779–811.
[12] Liu H, Wang M, Wang J. Monte Carlo simulations of gas flow and heat transfer in vacuum packaged MEMS devices. Appl Therm Eng 2007;27:323–9.
[13] Cia C. Heat transfer in vacuum package micro electromechanical system devices. Phys fluids 2008;20:017103.
[14] Rana A, Torrilhon M, Struchtrup H. Heat transfer in micro devices packaged in partial vacuum. J Phys Conf Ser 2012;362:012034.
[15] Wang QW, Zhao CL, Zeng M, Wu NYE. Numerical investigation of rarefied diatomic gas flow and heat transfer in microchannel using DSMC with heat flux specified boundary condition-part i: numerical method and validation. Numer Heat Flux Part B Fundam 2008;53:150–73.
[16] Wang QW, Zhao CL, Zeng M, Wu NYE. Numerical investigation of rarefied diatomic gas flow and heat transfer in microchannel using DSMC with heat flux specified boundary condition-part II: applications. Numer Heat Flux Part B Fundam 2008;53:174–87.
[17] Akhlaghi H, Roohi E, Stefanov S. A new iteration wall heat flux specifying technique in DSMC for heating/cooling simulations of MEMS/NEMS. Int J Therm Sci 2012;59:111–25.
[18] Bird GA. Molecular gas dynamics and the direct simulation of gas flow. Oxford: Oxford University Press; 1994.
[19] Mohammadzadeh A, Roohi E, Niazmand H, Stefsnov S, Myong RS. Thermal and second-law analysis of a micro- or nano-cavity using direct-simulation Monte Carlo. Phys Rev E 2012;85:056310.
[20] Ejtehadi O, Roohi E, Abolfazli J. Investigation of basic molecular gas structure effects on hydrodynamics and thermal behaviors of rarefied shear driven flow using DSMC. Int Commun Heat Mass Transf 2012;39:439–48.
[21] Amiri A, Rooh E, Niazmand H, Stefanov S. DSMC simulation of low Knudsen micro/nano flows using small number of particles per cells. J Heat Transf 2013;135:101008.
[22] Mohammadzadeh A, Roohi E, Niazmand H. A parallel DSMC investigation of monatomic/diatomic Gas flows in micro/nano cavity. Numer Heat Transf Part A Appl 2013;63:305–25.
[23] Akhlaghi H, Balaj M, Roohi E. Hydrodynamic behavior of micro/nanoscale Poiseuille flow under thermal creep condition. Appl Phys Lett 2013;103:073108.
[24] Balaj M, Roohi E, Akhlaghi H, Myong RS. Investigation of convective heat Transfer through constant wall heat flux micro/nano channels using DSMC. Int J Heat Mass Transf 2014;71C:633–8.
[25] Akhlaghi H, Roohi E. Mass flow rate prediction of thermal-pressure-driven Gas flows through micro-/nanoscale channels. Continuum Mech Thermodyn 2014;26:67–78.
[26] Akhlaghi H, Balaj M, Roohi E. A through study on thermal mass flux of rarefied flow through micro/nanochannels. Appl Phys Lett 2014;104:073109.